Soft Matter



View Article Online **PAPER**



Cite this: Soft Matter, 2022, 18.1219

Received 20th November 2021, Accepted 29th December 2021

DOI: 10.1039/d1sm01654q

rsc.li/soft-matter-journal

Lubricated soft normal elastic contact of a sphere: a new numerical method and experiment

An important problem in lubrication is the squeezing of a thin liquid film between a rigid sphere and an elastic substrate under normal contact. Numerical solution of this problem typically uses iteration techniques. A difficulty with iteration schemes is that convergence becomes increasingly difficult under increasingly heavy loads. Here we devise a numerical scheme that does not involve iteration. Instead, a linear problem is solved at every time step. The scheme is fully automatic, stable and efficient. We illustrate this technique by solving a relaxation test in which a rigid spherical indenter is brought rapidly into normal contact with a thick elastic substrate lubricated by a liquid film. The sphere is then fixed in position as the pressure relaxes. We also carried out relaxation experiments on a lubricated soft PDMS (polydimethysiloxane) substrate under different conditions. These experiments are in excellent agreement with the numerical solution.

1. Introduction

For engineering surfaces to operate smoothly and durably during contact it is often necessary to use a lubricant - typically a thin layer of oil — to reduce friction and adhesion. An important class of lubrication problems is when a coherent liquid film exists between two surfaces and the hydrodynamic pressure is sufficiently large to support a normal load without solid-solid contact. Elasto-hydrodynamic lubrication (EHL) is an important subclass of this problem in which the elastic deformation of at least one of the surfaces is significant.

Traditionally, the mechanics of stiff lubricated contacts such as metal bearings and pistons¹⁻³ has been studied using EHL theory. An excellent review of EHL theory can be found in the article by Zhu and Wang.4 EHL theory is also of fundamental importance to the understanding of filtration, coagulation and adhesion of small particles.^{5–7} In the tire industry, EHL theory governs how tires perform on a wet road.8,9 Recent interest in soft materials and bio-medical applications have expanded the use of EHL theory to study lubricated contact between a soft elastic solid and a hard surface and for contactless rheology. 10

For example, EHL theory has been used to study the lift forces of cylinders near compliant walls. 11,12

A conventional problem tackled by researchers in EHL is that of sliding. The standard approximation is to assume steady state conditions so the solution is independent of time. A numerical method for the point contact sliding problem was developed by Evans and Snidle, 13 who extended the inverse method first proposed by Dowson and Higginson¹⁴ for line contact. The essence of the approach is that, assuming a pressure field, the shape of the film is calculated in two different ways: one by elasticity and the second by inverting the Reynolds equation. The difference between the two calculated film shapes is used to iterate the actual pressure field, that is, the pressure is adjusted until the two shapes agree with each other.

Here we are interested in another fundamental problem which involves both time and space. This is the normal contact problem of squeezing a liquid film between two elastic surfaces. The line contact problem in which a thin liquid film between two infinite circular cylinders is squeezed by a normal force has been analyzed by many investigators. 15-17 The point contact problem, which involves lubricated normal contact of elastic surfaces, has been less studied. A seminal study of the point contact problem was carried out by Davis et al., 18 on the normal collision of two elastic spheres. Normal lubricated contact and sliding of rough surfaces have been studied by Persson and co-workers¹⁹⁻²¹ by a combination of random surface contact mechanics and lubrication theory. More recently, Wang et al.22 also developed a numerical method to study the deformation of elastic coatings under normal lubricated contact.

^a Field of Theoretical & Applied Mechanics, Department of Mechanical & Aerospace Engineering, Cornell University, Ithaca, NY 14853, USA. E-mail: ch45@cornell.edu

^b Department of Chemical and Biomolecular Engineering, 111 Research Drive, Lehigh University, Bethlehem, PA 18015, USA

^c Department of Bioengineering, 111 Research Drive, Lehigh University, Bethlehem, PA 18015, USA

^d Global Station for Soft Matter, GI-CoRE, Hokkaido University, Sapporo 001-0021,

[†] These authors contributed equally.

Our primary goal in this paper is to present a new numerical technique to solve the normal point contact problem. As in all EHL problems, the governing equation for flow is the Reynolds equation, which is highly nonlinear. This equation is coupled to elasticity via an integral equation which relates the elastic displacement to the hydrodynamic pressure. To the best of our knowledge, the numerical techniques designed to solve this coupled nonlinear problem all require iteration. These iteration procedures typically break down when the liquid film thickness is very small or pressure very high. Also, convergence can be very slow and involves many iterations. A common way to alleviate some of these difficulties is to use the inverse solution method first introduced by Dowson and Higginson.¹⁴ In this method, direct iteration is applied only in the low-pressure domain and the pressure is solved inversely in the high-pressure region. This method has been shown to be successful in handling high pressures. For example, Lee and Chang¹⁷ obtained the pressure and deformation profiles between two normally approaching lubricated cylinders using direct iteration in the low pressure (inlet) region and using Newton-Raphson to solve the nonlinear equation in the highpressure region. However, this procedure often requires manual adjustments, and the domain of high/low pressure can change continuously depending on the loading history. Hence, the method is not fully automatic. Likewise, in the point contact sphere collision problem, Davis et al. 18 reported that their iterative procedure breaks down when the elastic displacement of the colliding spheres is comparable to the initial film thickness. In their case, convergence in this regime is obtained using a relaxation technique. Again, this procedure usually requires manual adjustment of the relaxation parameter which differs from problem to problem. Recently, a new iterative numerical technique was developed by Wang et al.22 to study the deformation of elastic coatings under normal lubricated contact. In this scheme, the thickness of the liquid film is used as the iterant. Once it is specified, the pressure is computed by solving the Reynolds equation. The force acting on the indenter and the elastic displacement is then obtained using this pressure. From this displacement one can update the film thickness. In general, this updated film thickness does not satisfy force equilibrium; the film thickness is iterated until force balance

In this paper, we devise a novel numerical technique to solve the point contact problem without resorting to iteration. The numerical scheme boils down to solving a linear system of equations at each time step. The numerical scheme is stable, fast and can be solved using any standard matrix solver such as those in Matlab[®]. The solution scheme is fully automatic. We demonstrate this technique on the relaxation test. In this test, a rigid spherical indenter is brought close to contact with an elastic surface lubricated by a thin liquid film of initial minimum thickness z_0 . The indenter is then rapidly pushed down by a pre-determined amount d_c . The indenter's displacement is held fixed immediately after dc is reached. During this holding phase, flow reduces the hydrodynamic pressure and the elastic substrate rebounds. In this problem, the long-time force acting on the indenter depends on whether d_c/z_0 is less than or equal

Since we are primarily interested in soft lubricated contact, we focus on the case of constant viscosity. However, it has been known for a long time that at very high pressures, the viscosity of many lubricants increases rapidly with pressure. This phenomenon is very important for applications involving hard lubricated contact and can present additional numerical difficulty. A simple model for this dependence takes the form²³

$$\eta = \eta_0 e^{\alpha p} \tag{1}$$

where η_0 is the viscosity at ambient pressure and α is the viscosity-pressure coefficient. It should be noted that α is typically very small – it takes pressure on the order of hundreds of MPa for significant increase in viscosity. 23 Since the modulus of soft materials rarely exceeds a few MPa, there is little chance that this effect is relevant for soft contacts - the material will fail long before any substantial increase in viscosity.

The plan of this paper is as follows. Formulation of the point contact problem is summarized in Section 2. We then apply this formulation to model the relaxation problem. The experimental method for the relaxation test is described in Section 3. In Section 4 we highlight some simple analytical results on the relaxation test. These results provide physical insight and also serve as a check of our numerical method. In Section 5 we present a numerical scheme to solve the general point contact problem. We then apply this scheme to solve the special case of a relaxation test. Section 6 compares the numerical results with experimental data. This is followed by Summary and Discussion.

2. Problem formulation and geometry

The geometry consists of a rigid sphere of radius R lying above an elastic half space which is immersed in a fluid with viscosity η (Fig. 1). A cylindrical coordinate system (r, z) is used to specify position, with z = 0 corresponding to the undeformed surface of the elastic half space, which occupies z < 0. In the following, we make the usual approximation that deformation is restricted to a small region near the south pole of the sphere so that its surface can be approximated by a paraboloid. The

initial film thickness profile is defined by $h(r, t = 0) = z_0 + \frac{r^2}{2R^4}$

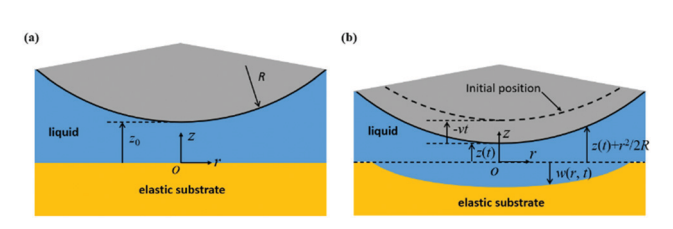


Fig. 1 (a) Geometry of a rigid sphere in lubricated contact with an elastic half space. The original position of the bottom of the sphere is at z_0 . (b) The sphere is pushed downwards with a constant velocity v. The solid line denotes the surface of the sphere at time t.

where $z_0 > 0$ denotes the initial position of the sphere bottom. At this position, the system is quiescent and there is no pressure acting on the substrate; as a result, the vertical displacement of the substrate, denoted by w(r, t), is zero everywhere. Here we have made the usual thin film approximation that the deformation is restricted to a small region near the south pole of the sphere so its surface can be approximated by a paraboloid. The substrate is assumed to be linearly elastic with Young's modulus E and Poisson's ratio ν .

We allow only vertical indenter motion, so the center of the sphere is directly above r = 0 and its position is completely specified by its vertical coordinate z(t). The liquid film thickness, h(r, t) is given by

$$h(r,t) = z(t) + \frac{r^2}{2R} - w(r,t).$$
 (2)

Note in our coordinate system, $w(r, t) \leq 0$ for positive pressure. The axisymmetric Reynolds equation for hydrodynamic lubrication in cylindrical coordinates is:²⁴

$$\frac{\partial h}{\partial t} = \frac{1}{12r} \frac{\partial}{\partial r} \left(\frac{rh^3}{\eta} \frac{\partial p}{\partial r} \right),\tag{3}$$

where p is the hydrodynamic pressure and h is given by eqn (2). To evaluate the gap or film thickness h in eqn (2), one needs the elastic displacement w which is related to the pressure by:²⁵

$$w(r,t) = \frac{-4}{\pi E^*} \int_0^\infty \frac{u}{u+r} p(u,t) K \left[\frac{4ru}{(u+r)^2} \right] du, \tag{4}$$

where $E^* = E/(1 - \nu^2)$ is the plane strain modulus of the half space and *K* is the complete elliptical integral of the first kind. Eqn (2)-(4) are the governing equations for EHL for our geometry.

2.1. Special case: relaxation test

An example of a point contact problem that has not been previously studied is the relaxation test. In this test, the sphere represents the tip of a rigid indenter. At time t = 0, it starts to move downwards at a fixed speed v_0 until $t = t_c$ (loading phase). At the end of the loading phase the indenter has travelled a distance $d_c = v_0 t_c$. After $t_c = d_c / v_0$ the indenter position is fixed (hold phase). Specifically, the evolution of zin eqn (1) is:

$$z(t) = \begin{cases} z_0 - v_0 t & 0 \le t \le t_c \\ z_0 - d_c & t_c \le t \end{cases}$$
 (5a, b)

The boundary condition is that the pressure vanishes at $r = \infty$ and $\frac{\partial p}{\partial r} = 0$ at the origin. The latter condition reflects the fact that, because our domain is axisymmetric, we expect the pressure field to have a local extremum at r = 0. The initial condition for the loading phase is

$$z(t=0) = z_0 \tag{6a}$$

$$\frac{\mathrm{d}z}{\mathrm{d}t}(t=0) = -v_0 \tag{6b}$$

2.2. Normalization

We introduce the following normalization to expedite analysis:

$$\bar{r} = r / \sqrt{Rd_c},$$
 (7a)

$$\bar{h} = h/d_{\rm c},$$
 (7b)

$$\bar{t} = t/t_{\rm c},\tag{7c}$$

$$\bar{z} = z/d_{\rm c},$$
 (7d)

$$\bar{w} = w/d_{\rm c},\tag{7e}$$

$$\bar{p} = \frac{\pi}{2E^*} \sqrt{\frac{R}{d_c}} p \tag{7f}$$

Here a bar denotes a dimensionless quantity. Substituting eqn (7a)-(7f) into eqn (2)-(5) and assuming a constant viscosity $\eta = \eta_0$ results in

$$\frac{\partial \bar{h}}{\partial \bar{t}} = \frac{\beta}{r} \frac{\partial}{\partial \bar{r}} \left(\bar{r} h^{\bar{3}} \frac{\partial \bar{p}}{\partial \bar{r}} \right), \quad \bar{h} = \bar{z} + \frac{\bar{r}^2}{2} - \bar{w}$$
 (8a)

$$\bar{w} = -\frac{8}{\pi^2} \int_0^\infty \frac{\bar{u}}{\bar{u} + \bar{r}} \, \bar{p}(\bar{u}, \bar{t}) K \left(\frac{4\bar{u}\bar{r}}{(\bar{u} + \bar{r})^2} \right) d\bar{u} \tag{8b}$$

$$\bar{z}(\bar{t}) = \begin{cases} \bar{z}_0 - \bar{t} & 0 \le \bar{t} < 1\\ \bar{z}_0 - 1 & \bar{t} \ge 1 \end{cases}$$
 (8c, d)

where

$$\beta \equiv \frac{E^* d_{\rm c}^{5/2}}{6\pi\eta_0 v_0 R^{3/2}},\tag{8e}$$

$$\bar{z}_0 = z_0/d_c \tag{8f}$$

The initial conditions eqn (6a) and (6b) become:

$$\bar{z}(\bar{t}=0)=\bar{z}_0,\tag{9a}$$

$$\frac{\mathrm{d}\bar{z}}{\mathrm{d}\bar{t}}\Big|_{\bar{t}=0} = -1. \tag{9b}$$

Using eqn (8a) and eqn (8c), (8d), the normalized partial differential equations (PDEs) for the loading and holding phase are:

$$-1 - \frac{\partial \bar{w}}{\partial \bar{t}} = \frac{\beta}{\bar{r}} \frac{\partial}{\partial \bar{r}} \left(\bar{r} \left(\bar{z}_0 - \bar{t} + \frac{\bar{r}^2}{2} - \bar{w} \right)^3 \frac{\partial \bar{p}}{\partial r} \right)$$

$$\bar{t} < 1 \text{ (loading)}$$
(10a)

$$-\frac{\partial \bar{w}}{\partial \bar{t}} = \frac{\beta}{\bar{r}} \frac{\partial}{\partial \bar{r}} \left(\bar{r} \left(\bar{z}_0 - 1 + \frac{\bar{r}^2}{2} - \bar{w} \right)^3 \frac{\partial \bar{p}}{\partial \bar{r}} \right) \quad \bar{t} > 1 \text{ (hold)} \quad (10b)$$

For the hold phase, we impose continuity of pressure and displacement field at $\bar{t} = 1$. The boundary conditions for both eqn (10a) and (10b) are that the pressure vanishes at infinity and $\frac{\partial p}{\partial \bar{r}} = 0$ at the origin.

The force F during relaxation is computed by integrating the pressure field and is

$$F(t) = 2\pi \int_0^\infty p(r, t) r dr.$$
 (11a)

Using the normalization scheme eqn (7a)–(7f), the normalized force \bar{F} is

$$F \equiv \frac{2E^* d_c^{3/2} \sqrt{R}}{\pi} \bar{F} \Rightarrow \bar{F} = 2\pi \int_0^\infty \bar{p}(\bar{r}, \bar{t}) \bar{r} d\bar{r}. \tag{11b}$$

Eqn (10a) and (10b) imply that the solution of the relaxation problem depends on two dimensionless parameters, \bar{z}_0 and β . Let us consider the physical meaning of these parameters. In a relaxation test, $\bar{z}_0 = z_0/d_c > 1$ means indentation is smaller than the initial separation between the spherical indenter and the soft substrate. This means that it is not possible to drain the fluid underneath the indenter sufficiently to establish solid/ solid contact. For this case, flow will continue until pressure vanishes everywhere during the hold phase. This results in the indentation force approaching zero at long times. On the other hand, when $\bar{z}_0 < 1$, indentation is large enough so all the fluid underneath the indenter is eventually drained. For this case, the indentation force is non-zero at long times. The parameter β in eqn (8e) is the ratio of flow velocity generated by hydrodynamic pressure which scales with $\eta_0^{-1}R^{-1}E^*d_c^2$ to the flow velocity cause by indentation, ²⁶ i.e., $v_0 \sqrt{R/d_c}$. Physically, large indentation speed, high viscosity, soft substrate and small indentation reduce flow and hence decrease β . In the following we will explore more precisely how some of these parameters control the relaxation process. Here we give an estimate of β for soft materials. The indenter speed v_0 can vary by several orders of magnitude in an experiment, typically from 1 μm s⁻¹ to 1 mm s⁻¹. For soft solids such as PDMS the plane strain modulus $E^* \sim 4 \times 10^6$ Pa. For a moderately viscous liquid, $\eta \approx 0.1$ Pa s. Taking R = 1 mm, $d_c = 10$ µm, we find $10 \le \beta \le 10^4$. For very stiff solids such as metals, β can be extremely large, since E^* can be six orders of magnitude higher. In this case, other assumptions such as isoviscosity (see eqn (1)) and incompressibility of the lubricant, are often inaccurate.

3. Materials and methods

3.1. Sample fabrication

Poly(dimethylsiloxane) (PDMS) samples about 2 cm \times 2 cm \times 5 mm were fabricated based on a silicone elastomer kit (DOW SYLGARD 184, DOW Corning). The elastomer base and curing agent were mixed in a ratio of 10:1, and the mixture was cured for 2 hours at 80 $^{\circ}$ C.

3.2. Relaxation experiment

Load on and displacement of an indenter made of a glass bead (2 mm radius, McMaster-Carr) indenting a flat lubricated PDMS sample were measured and recorded by a custom-built flat-on-flat tribometer (see ref. 26 for description). The PDMS strip as prepared was mounted on the flat-on-flat tribometer and

silicone oil (100 Pa s at 25 °C, Sigma-Aldrich) that served as lubricant was added on the top surface of the PDMS sample. After adding lubricant, the indenter was slowly (0.001 mm s⁻¹) brought down until the indenter contacted the sample, as detected by a load cell. Then the indenter was lifted up a distance of 140 µm (*i.e.*, $z_0 = 140$ µm), and the system was allowed to relax for a few minutes. This was followed by moving the indenter rapidly downward at a constant velocity of 0.1 mm s⁻¹ for (a) 126 µm ($z_0/d_c = 1.11$), (b) 140 µm ($z_0/d_c = 1$), or (c) 154 µm ($z_0/d_c = 0.91$). Indenter motion was then halted abruptly and the indenter was subsequently held in place. The normal force and the position of the indenter were recorded during this process as a function of time. Based on collected data, the corresponding β , \bar{t} and \bar{F} were calculated and compared with numerical solutions.

Behavior of the solution in different regimes

Before diving into numerical methods and calculations, we discuss several special cases where approximate solutions can be obtained. These solutions give physical insight on the relaxation process and serve as a check of our numerical method.

4.1. Asymptotic solution for large β

As noted above, β is typically much greater than one. For this case, eqn (10a) suggests looking for a solution where the pressure is of order $1/\beta$. Hence, the displacement of the substrate is also of order $1/\beta$ and can be ignored relative to $\bar{z} + \frac{\bar{r}^2}{2}$. Substituting $\bar{p} \equiv \hat{p}(\bar{r}, \bar{t})/\beta$ into eqn (10a) and keeping only leading order terms, eqn (10a) becomes:

$$-\frac{\mathrm{d}\bar{z}}{\mathrm{d}\bar{t}} = \frac{1}{\bar{r}}\frac{\partial}{\partial \bar{r}} \left(\bar{r} \left(\bar{z}(t) + \frac{\bar{r}^2}{2} \right)^3 \frac{\partial \hat{p}}{\partial r} \right) \quad \bar{t} < 1$$
 (12a)

Eqn (12a) can be integrated with respect to the spatial coordinate; the resulting hydrodynamic pressure is

$$\bar{p} = \frac{\dot{\bar{z}}}{4\beta} \left(\bar{z}(\bar{t}) + \frac{\bar{r}^2}{2} \right)^{-2} \tag{12b}$$

where $\dot{z} \equiv d\bar{z}/d\bar{t}$. Note this solution is valid only for short times or sufficiently low pressure where elasticity can be neglected. For example, the pressure given by eqn (12b) depends on \bar{z} – it becomes unbounded at the origin $\bar{r}=0$ as $\bar{z}\to 0$. Indeed, for $\bar{z}_0<1$ (large indentation), the pressure predicted by eqn (12b) becomes unbounded at $\bar{r}=0$ as $\bar{t}\to 1$ since $\bar{z}=\bar{z}_0-\bar{t}$ reaches zero at $\bar{t}=\bar{z}_0<1$ (recall that holding occurs at $\bar{t}\geq 1$). Thus, for large indentations, eqn (12b) is valid only for short times $\bar{t}<1$. On the other hand, for small indentations where $\bar{z}_0>1$, the pressure given by eqn (12b) is valid for the entire loading phase provided that $\beta\gg 1$. For this case, eqn (12b) can be used as the initial condition for eqn (10b).

4.2. Long time solution for the relaxation problem

Relaxation is governed by eqn (10b). Here we note that a natural time scale in the holding phase is obtained by renormalizing time t as $\tilde{t} = \beta M x \bar{0} 074$; $= \beta t/t_c \equiv t/t_R$ where $t_R \equiv \frac{6\pi \eta_0 R^{3/2}}{E^* d_c^{3/2}} = t_c/\beta$. Later we shall see that t_c is the characteristic relaxation time.

Later, we shall see that $t_{\rm R}$ is the characteristic relaxation time. With this new normalization, eqn (10b) is:

$$-\frac{\partial \bar{w}}{\partial \tilde{t}} = \frac{1}{\bar{r}} \frac{\partial}{\partial \bar{r}} \left(\bar{r} \left(\bar{z}_0 - 1 + \frac{\bar{r}^2}{2} - \bar{w} \right)^3 \frac{\partial \bar{p}}{\partial r} \right) \quad \tilde{t} > \beta$$
 (13)

Consider first the regime of large indentation where $\bar{z}_0 < 1$. In this regime, we expect most of the fluid will be squeezed out at long times and the pressure field is given by the classical Hertz theory:²⁵

$$\bar{p}(\bar{r}, \tilde{t} \to \infty) = \begin{cases} \sqrt{(1 - \bar{z}_0) - \bar{r}^2} & \bar{r} < \bar{r}_\infty \equiv \sqrt{1 - \bar{z}_0} \\ 0 & r > \bar{r}_\infty \end{cases}$$
(14)

where $\bar{r}_{\infty} \equiv \sqrt{1 - \bar{z}_0}$ is the normalized contact radius. Mathematically, this can be seen by noting that

$$h(\bar{r} < \bar{r}_{\infty}, \tilde{t} \to \infty) = \bar{z}_0 - 1 + \frac{\bar{r}^2}{2} - \bar{w} = 0 \Rightarrow \bar{w} = -\left(1 - \bar{z}_0 - \frac{\bar{r}^2}{2}\right)$$
(15)

is the Hertz contact condition and satisfies eqn (13) exactly for $\bar{r} < \bar{r}_{\infty}$. Thus, for $\bar{z}_0 < 1$, the long-time indenter force is positive and should plateau to (using Hertz theory and eqn (11a) and (11b))

$$F_{\infty} = \frac{4E^*\sqrt{R}}{3}(d_{\rm c} - z_0)^{3/2} \Rightarrow \bar{F}_{\infty} = \frac{2\pi}{3}(1 - \bar{z}_0)^{3/2}$$
 (16)

The situation is more complicated for $\bar{z}_0 > 1$. There is no simple analytical solution for the long-time pressure distribution other than the fact that it decays to zero everywhere so $F_{\infty}=0$. The behavior in this regime will be explored numerically in Sections 5 and 6.

5. Numerical method

In the following, we focus on the numerical solution of the general case where h is given by eqn (2). Without loss of generality, we use the same normalization as eqn (7a)–(7f), except that time t is normalized by T, i.e., $\bar{t}=t/T$, where T is a characteristic time in the problem. T varies from problem to problem. For example, in the relaxation problem, $T=z_0/v_0=t_c$. We discretize time into equal steps, $\bar{t}_j=j\Delta\bar{t},\ j=0,\ 1,\ldots$ We replace the infinite interval $\bar{r}\in[0,\ \infty)$ by a finite interval $\bar{r}\in[0,\ \bar{L}]$ and discretize it into N equally spaced points $r_i,\ i.e.,\ \bar{r}_{i+1}=\bar{r}_i+\Delta\bar{r},\ 1\leq i\leq N$. Denote solution at time step j at \bar{r}_i to

be \bar{p}_{i}^{j} . The differential equation eqn (8a) can be written as:

$$-\frac{\partial \bar{w}}{\partial \bar{t}} = -\frac{\mathrm{d}\bar{z}}{\mathrm{d}\bar{t}} + \beta \left([m(\bar{r},\bar{t})]^{3} \frac{\partial^{2}\bar{p}}{\partial \bar{r}^{2}} \right)$$

$$+ \beta \left(3[m(\bar{r},\bar{t})]^{2} \left(\bar{r} - \frac{\partial \bar{w}}{\partial \bar{r}} \right) \frac{\partial \bar{p}}{\partial \bar{r}} \right)$$

$$+ \beta \left(\frac{1}{\bar{r}} [m(\bar{r},\bar{t})]^{3} \frac{\partial \bar{p}}{\partial \bar{r}} \right)$$

$$(17a)$$

where $m(\bar{r}, \bar{t}) \equiv \bar{z}(\bar{t}) + \frac{\bar{r}^2}{2} + \bar{w}$. The 1st and 2nd spatial derivatives of pressure at time step j + 1 are computed using

$$\left. \frac{\partial^2 \bar{p}}{\partial \bar{r}^2} \right|_{i+1} = \frac{\bar{p}_{i+1}^{j+1} - 2\bar{p}_i^{j+1} + \bar{p}_{i-1}^{j+1}}{\left(\Delta \bar{r}\right)^2},\tag{17b}$$

$$\frac{\partial \bar{p}}{\partial \bar{r}}\Big|_{i+1} = \frac{\bar{p}_{i+1}^{j+1} - \bar{p}_{i}^{j+1}}{\Delta \bar{r}},\tag{17c}$$

The time derivative is computed using:

$$\left. \frac{\partial \bar{w}}{\partial \bar{t}} \right|_{i+1} = \frac{\bar{w}_i^{j+1} - \bar{w}_i^j}{\Delta \bar{t}},\tag{18a}$$

$$\frac{\mathrm{d}\bar{z}}{\mathrm{d}\bar{t}}\Big|_{i+1} = \frac{\bar{z}^{i+1} - \bar{z}^{i}}{\Delta\bar{t}} \tag{18b}$$

This is a backward Euler discretization that is first-order accurate and due to its implicit nature provides greater numerical stability compared to an explicit Euler discretization. The key is to avoid solving a nonlinear equation, thus negating the need to iterate which is the main source of difficulty. This is accomplished by evaluating $m(\bar{r}, \bar{t})$ and the spatial derivative of displacement at the previous time step j, i.e.,

$$\left(\bar{z}^j + \frac{\bar{r}_i^2}{2} - \bar{w}_i^j\right) \equiv m_i^j \tag{19a}$$

and

$$\frac{\partial \bar{w}}{\partial \bar{r}} = \frac{\bar{w}_{i+1}^j - \bar{w}_i^j}{\Delta \bar{r}} \tag{19b}$$

where $\bar{z}^j \equiv \bar{z}(t_j)$. This hybrid method preserves stability and allows us to solve a linear problem at each time step. After some algebra, the discretized version of eqn (17a) is

$$-\frac{(\Delta \bar{r})^{2}}{\beta \Delta \bar{t}} w_{i}^{j+1} + \left[2(m_{i}^{j})^{3} + (m_{i}^{j})^{2} n_{i}^{j} \Delta \bar{r} \right] \bar{p}_{i}^{j+1}$$

$$- \left[(m_{i}^{j})^{3} + (m_{i}^{j})^{2} n_{i}^{j} \Delta \bar{r} \right] \bar{p}_{i+1}^{j+1}$$

$$- (m_{i}^{j})^{3} \bar{p}_{i-1}^{j+1} = -(\bar{w}_{i}^{j} + \bar{z}^{j+1} - \bar{z}^{j}) \frac{(\Delta \bar{r})^{2}}{\beta \Delta \bar{t}} \quad 2 \leq i \leq N - 1$$
(20a)

where

$$n_i^j \equiv 3\left(\bar{r}_i - \frac{w_{i+1}^j - w_i^j}{\Delta \bar{r}}\right) + \frac{m_i^j}{\bar{r}_i}.$$
 (20b)

Paper Soft Matter

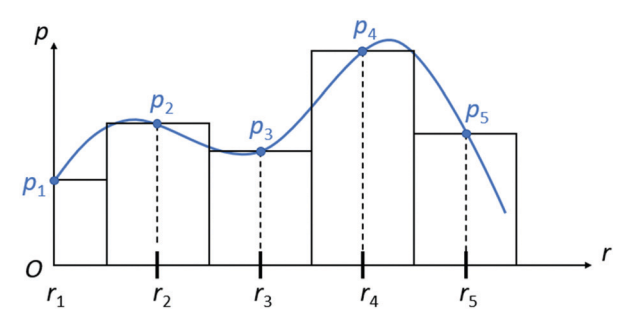


Fig. 2 Discrete pressure distribution within each spatial step is used to create the algebraic set of equations.

In order to evaluate the displacement field \bar{w}^j at time step j, we assume the pressure distribution within the domain $[\bar{r}_m - \Delta \bar{r}/2,$ $\bar{r}_m + \Delta \bar{r}/2$] is uniform and equal to \bar{p}_m^j , where $2 \leq m \leq N$ (Fig. 2). Within the domain $[0, \Delta \bar{r}/2]$, the pressure is \bar{p}_1^j .

The integral connecting pressure to displacement field eqn (8b), is evaluated numerically according to:

$$\bar{w}_{i}^{j+1} = -\frac{8}{\pi^{2}} \int_{0}^{\Delta \bar{r}/2} \frac{\bar{u}}{\bar{u} + \bar{r}_{i}} \bar{p}_{1}^{j+1} K \left(\frac{4\bar{u}\bar{r}_{i}}{(\bar{u} + \bar{r}_{i})^{2}} \right) d\bar{u}
- \frac{8}{\pi^{2}} \sum_{m=2}^{N} \int_{\bar{r}_{m} - \Delta \bar{r}/2}^{\bar{r}_{m} + \Delta \bar{r}/2} \frac{\bar{u}}{\bar{u} + \bar{r}_{i}} \bar{p}_{m}^{j+1} K \left(\frac{4\bar{u}\bar{r}_{i}}{(\bar{u} + \bar{r}_{i})^{2}} \right) d\bar{u}$$

$$= -\hat{w}_{i1} \bar{p}_{1}^{j+1} - \sum_{m=2}^{N} \hat{w}_{im} \bar{p}_{m}^{j+1}$$
(21a)

where

$$\hat{w}_{i1} \equiv \frac{8}{\pi^2} \int_0^{\Delta r/2} \frac{\bar{u}}{\bar{u} + \bar{r}_i} K\left(\frac{4\bar{u}\bar{r}_i}{\bar{u}(\bar{u} + \bar{r}_i)^2}\right) d\bar{u}, \tag{21b}$$

$$\hat{w}_{im} \equiv \frac{8}{\pi^2} \int_{\bar{r}_m - \Delta r/2}^{\bar{r}_m + \Delta r/2} \frac{\bar{u}}{\bar{u} + \bar{r}_i} K\left(\frac{4\bar{u}\bar{r}_i}{\bar{u}(\bar{u} + \bar{r}_i)^2}\right) d\bar{u}$$
 (21e)

It is important to note that \hat{w}_{i1} and \hat{w}_{im} in eqn (21b) and (21c) are independent of pressure and surface displacement and hence need to be determined only once and stored as a vector. This further speeds up the numerical procedure. Physically, \hat{w}_{im} are influence coefficients for the displacement at a field point due to the pressure at a source point. The boundary conditions

are:
$$\frac{\partial \bar{p}}{\partial \bar{r}}\Big|_{\bar{r}=0} = \frac{\bar{p}_2^j - \bar{p}_1^j}{\Delta r} = 0$$
 and $\bar{p}_{i=N}^j = 0$. The cylindrical coordinate

system causes a singularity at the origin $(r = r_1 = 0)$ (see eqn (8a)). Here we bypass this difficulty since eqn (20a) is for $2 \le i \le N-1$. We simply enforce boundary conditions using

$$\bar{p}_1^j = \bar{p}_2^j \tag{22a}$$

$$\bar{p}_{i=N}^j = 0 \tag{22b}$$

Eqn (20a), (21a), (22a) and (22b) constitute a linear system of equations for the pressure and displacement in the (j + 1)th time step once the pressure and displacement in the *i*th time step are known. No iteration is needed. The matrix associated with this linear system of equations is given in the Appendix.

It should be noted that in many applications, e.g., in the relaxation problem considered in this work, \bar{z} is a known function of time so $d\bar{z}/d\bar{t}$ can be evaluated exactly so the discretization eqn (18b) is not necessary. In certain cases, such as the collision problem of Davis, \bar{z} is determined by solving two first order linear ordinary differential equations (ODEs) in time.

In our numerical technique, one starts the simulations with \bar{z}^1 , \bar{p}_i^1 (\bar{w}_i^1 can be found using eqn (21a)). The initial position of the indenter/sphere, \bar{z}^1 , is known from initial condition. In many problems, the system is initially quiescent, with zero pressure everywhere. However, for the relaxation problem, there is a sudden pressure jump at $t = 0^+$ as indicated by eqn (12). For $\beta \gg 1$ and for initial film thickness that is large in comparison with elastic displacement, an excellent choice for \bar{p}_i^1 is to use eqn (12b). For this case, the error will be small even if one use $\bar{p}_i^1 = 0$ since these conditions imply small pressure $(\sim 1/\beta)$. However, eqn (12b) should not be used if these conditions are not met, for example, if β is not large. A simple way to bypass this issue is to ramp the velocity of the indenter or sphere quickly from 0 to v_0 , which is exactly what is done in real life. This can be accomplished by starting the simulation at an earlier time, $t = -t_1 < 0$ when the system is quiescent so $p(r, t = -t_1) = 0$ and define

$$z(t) = z_0 - \left(t + \frac{t^2}{2t_1}\right)$$
 for $-t_1 \le t \le 0$ (23)

6. Special case: relaxation test

Convergence test

We apply our numerical scheme to simulate the relaxation test. First, we carried out a convergence test by changing the element size (Δr) and time step size (Δt) or domain size (L). Fig. 3 plots the pressure distribution at the end of the relaxation test for a large indentation test where $\bar{z}_0 = 0.5$ for different meshes, time steps and domain sizes. Note that our choice of $\bar{z}_0 = 0.5$ implies that the elastic displacement is twice of the initial thickness of

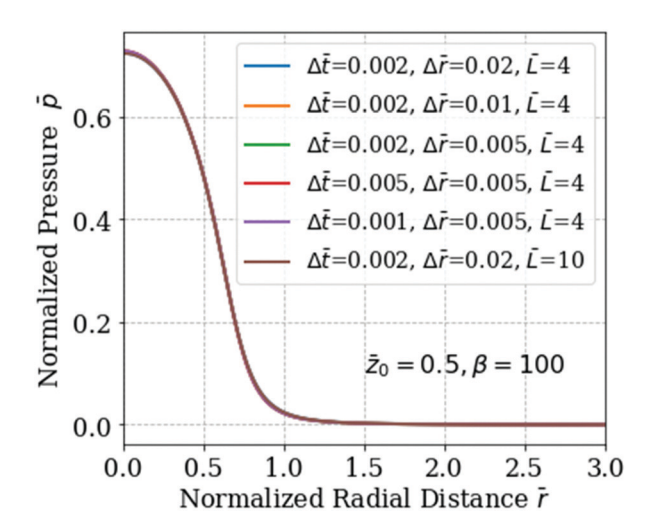


Fig. 3 Pressure distribution at the end of the relaxation test for a large indentation test where $\bar{z}_0 = 0.5$ for different mesh, time step and domain sizes.

the fluid layer, yet we have encountered no numerical difficulties. The numerical solutions lie right on top of each other. In the following calculations, we will use $\Delta \bar{r} = 0.01$, $\Delta \bar{t} = 0.001$ and $\bar{L} = 4$.

6.2. Results: relaxation test

Fig. 4a-c plot the pressure distribution for different normalized indentation depths \bar{z}_0 and normalized time \bar{t} for β = 100. The pressure in the loading phase ($\bar{t} \leq 1$) is shown by solid lines. For the holding phase where $\bar{t} > 1$, pressure distributions are indicated by dashed lines. For large indentation, $\bar{z}_0 = 0.5$, the short time and long-time asymptotic solutions are shown for comparison. In this case the long-time pressure distribution matches the Hertzian profile (eqn (14)), as expected. For small indentation where $\bar{z}_0 = 2$ (Fig. 4b and c), pressure increases transiently and then decays rapidly to zero in the hold phase (at the time scale of $t_R = \beta^{-1}t_c$, $\bar{t} = 10$ in Fig. 4c corresponds to t = 10 $10t_c = t_R/10$). A further check of our numerical scheme is to compare the long-time pressure with the Hertz pressure eqn (14) which is indicated by the black symbols (o). If our numerical scheme is accurate, the long-time pressure for $\bar{z}_0 < 1$ should converge to the Hertz pressure for long times, which is the case in Fig. 4a. Fig. 5a-c show the film thickness profile for different indentations at different times. As expected, for small indentation depths ($\bar{z}_0 \ge 1$, Fig. 5b and c), a thin layer of fluid remains on the entire interface. However, for indentation depths $\bar{z}_0 < 1$ (Fig. 5a, $\bar{z}_0 = 0.5$), most of the fluid in the pocket formed by the deformation of the elastic substrate has been squeezed out by \bar{t} = 5. The surface displacement of the substrate for different indentation depths at different times is shown in Fig. 6a-c. For small indentation depths $\bar{z}_0 \geq 1$, Fig. 6(b and c), the substrate surface rebounds to its original flat state for $\bar{t} \geq 5$. This is not the case for larger indentation depths where $\bar{z}_0 < 1$. For these cases, the Hertz pressure causes permanent substrate deformation (Fig. 6a).

6.3. Comparison between experiment results and numerical solution

As a further check on our numerical solution and lubrication model, we performed relaxation experiments as described in the Materials and methods section. To compare experimental and simulation results, we converted dimensionless variables to dimensional values based on eqn (7a)-(7f) and (11a), (11b). Fig. 7a-c show the comparison between numerical solution and experimental results for a fluid viscosity of 100 Pa s (as provided by the manufacturer) and Young's modulus of 2.94 MPa, a reasonable value for Sylgard-184 PDMS. Since PDMS is almost incompressible, we set $\nu = 0.5$. It is evident that experiments and numerical solutions are in excellent agreement.

7. Discussion and conclusion

We developed a new numerical scheme to solve lubricated normal elastic point contact problems. We applied this numerical technique to simulate a relaxation test. We provide simple analytic expressions for short- and long-time behavior. We also conducted relaxation experiments on a glass (indenter)/silicone oil (lubricant)/PDMS (substrate) system to test our model and numerical scheme. We found excellent agreement between our numerical solution and experimental data. Our numerical method is stable, highly efficient and fully automatic.

The geometry in this paper is mathematically equivalent to the normal lubricated contact of two elastic spheres provide that R in (1) is replaced by the reduced radius which is related to the radii of the spheres R_1 and R_2 by 25 $R^{-1} = R_1^{-1} + R_2^{-1}$. Likewise, the plane strain modulus E^* of the half space in (3) should be replaced by the reduced modulus:

$$1/E^* \to E_1^{-1}(1-\nu_1^2) + E_2^{-1}(1-\nu_2^2),$$
 (24)

where E_i , ν_i are the Young's moduli and Poisson's ratios of the spheres. With these simple modifications, our numerical method can be used to analyze lubricated contact of elastic spheres. Also, with a bit of effort, one can use a variable-size mesh (e.g., a finer mesh at the location of large pressure gradient) or variable time steps.

The numerical method used in this work assumes a constant time step and a uniform spatial mesh which is easy to implement but less efficient. In some problems, it may be useful to modify this technique to variable time stepping and non-uniform spatial meshing. Such modifications are rather straightforward. Another improvement is to change the current time stepping method to more accurate integration schemes

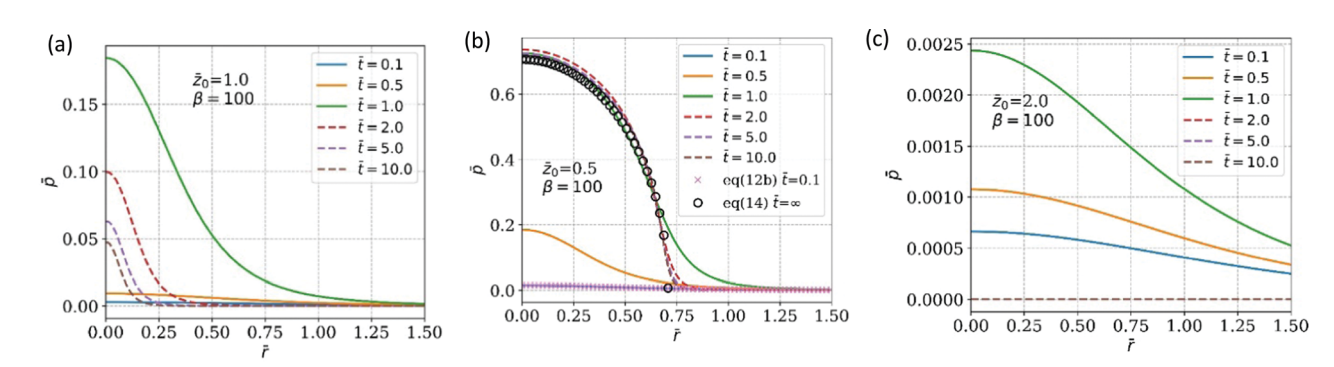


Fig. 4 Normalized pressure distribution as a function of normalized time for different indentation depths. Results during loading phase ($\tilde{t} \le 1$) are shown by solid lines. Results during holding phase ($\bar{t} > 1$) are shown by dashed lines. (a) Large indentation: $\bar{z}_0 = 0.5$; symbols (short time (x), long time (o)) are asymptotic results (eqn (12b) and (14)). (b) transition case: $\bar{z}_0 = 1$ (c) small indentation: $\bar{z}_0 = 2$.

Paper Soft Matter

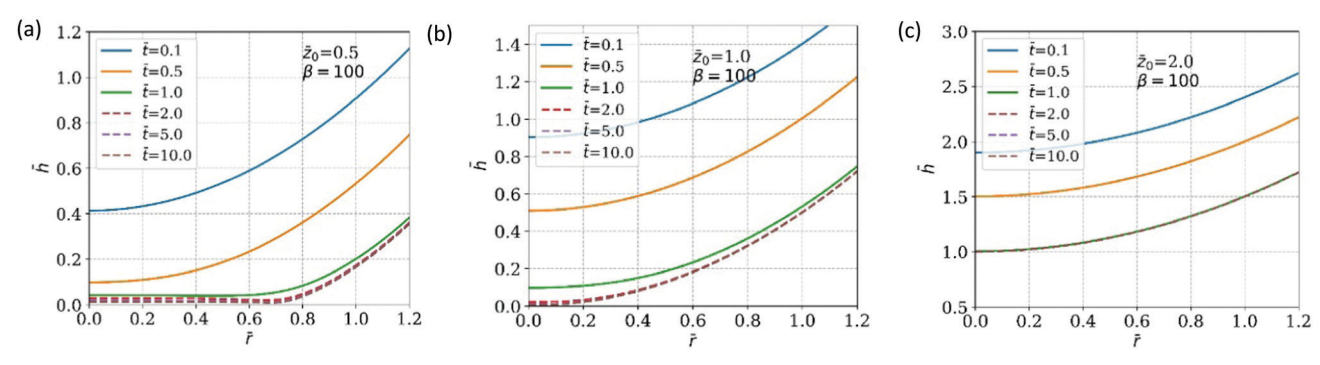


Fig. 5 Normalized liquid film thickness profile as a function of normalized time. Time profiles during loading phase ($\bar{t} \le 1$) are shown by solid lines. Profiles during holding phase ($\bar{t} > 1$) are shown by dashed lines. (a) Large indentation: $\bar{z}_0 = 0.5$, (b) transition case: $\bar{z}_0 = 1$ (c) small indentation: $\bar{z}_0 = 2.5$

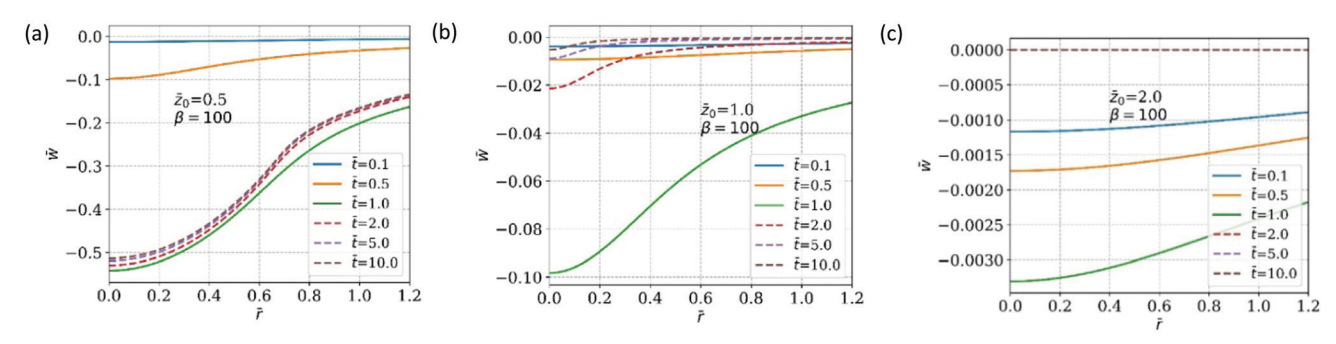


Fig. 6 Normalized substrate surface displacement profile at different times. Results during loading phase ($\bar{t} \le 1$) are given by solid lines. Results during holding phase ($\bar{t} > 1$) are given by dashed lines. (a) Large indentation: $\bar{z}_0 = 0.5$, (b) Transition case: $\bar{z}_0 = 1$ (c) Small indentation: $\bar{z}_0 = 2$.

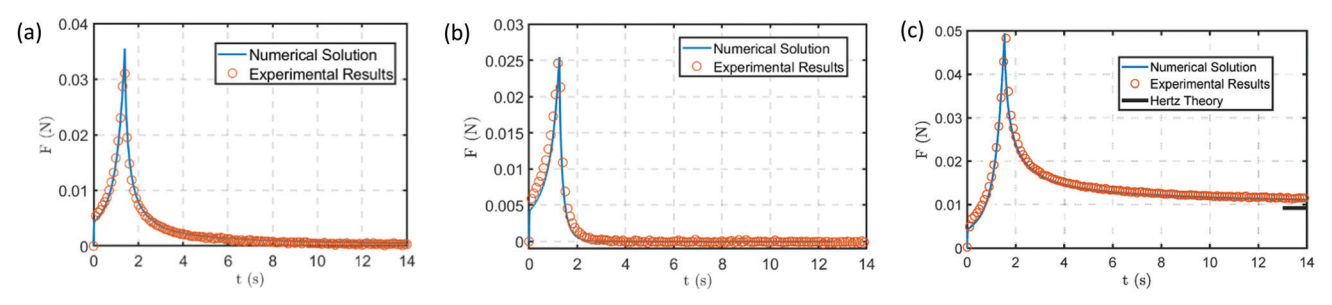


Fig. 7 Comparison between numerical solution and experimental results based on 100 Pa s silicone oil and PDMS Young's modulus of 2.94 MPa for (a) $z_0/dc = 1.0$, (b) $z_0/dc = 1.11$, and (c) $z_0/dc = 0.91$. The short black line on the right-hand side shows the fully-relaxed solution for force given by eqn (16).

such as the Runge–Kutta methods. In this way one can take larger time-steps. Also, it is not difficult to generalize our numerical method to include pressure dependent viscosity. In addition, since the Green's function for elastic substrate with finite thickness is known, ²⁷ our numerical scheme can be easily modified to account for an elastic substrate with finite thickness. This method can also be extended to study viscoelastic substrates. As noted in the Introduction, there is considerable interest in problems where the surfaces are not smooth. Our numerical formulation should readily accommodate spatially varying surface profiles and be applicable to this class of problems. Other EHL problems such as lubricated sliding of a sphere can be more difficult to solve because of increased complexity such as loss of axisymmetry. These modifications and extensions will be studied in future works.

Author contributions

Z. Liu worked on derivation of the numerical method and its implementation, and co-wrote the manuscript. H. Dong designed and conducted the experiments and their comparison with model results. A. Jagota designed the experiments, analysed results, and contributed to the manuscript. C.-Y. Hui conceived the idea, derived the method, and co-wrote the manuscript.

Conflicts of interest

There are no conflicts of interest to declare.

Appendix

Equations (20a) and (21a), along with the boundary conditions (22a,b), form a linear system of equations. In matrix form:

where

$$A_{i}^{j} = 2(m_{i}^{j})^{3} + (m_{i}^{j})^{2} n_{i}^{j} \Delta \bar{r}, \quad B_{i}^{j} = (m_{i}^{j})^{3} + (m_{i}^{j})^{2} n_{i}^{j} \Delta \bar{r}, \quad C_{i}^{j} = (m_{i}^{j})^{3}, \quad E_{i}^{j} = -\frac{(\Delta \bar{r})^{2}}{\beta \Delta \bar{t}} w_{i}^{j}, \quad D = -\frac{(\Delta \bar{r})^{2}}{\beta \Delta \bar{t}}, \quad (A2a-e)$$

Acknowledgements

This work was supported by a grant from the National Science Foundation through Grant LEAP-HI: CMMI-1854572.

References

- 1 A. Grubin, Investigation of the Contact Machine Components, Book No. 30, Central Scientific Research Institute for Technology and Mechanical Engineering, Moscow (DSIR Translation), 1949, vol. 2, pp. 115-166.
- 2 E. K. Gatcombe, Trans. ASME, 1945, 67, 177.
- 3 D. Dowson, Engineering, 1961, 192, 158.
- 4 D. Zhu and Q. Wang, J. Tribol., 2011, 133, 1-14.
- 5 N. A. Esmen, P. Ziegler and R. Whitfield, J. Aerosol Sci., 1978, 9, 547-556.
- 6 T. D'Ottavio and S. L. Goren, Aerosol Sci. Technol., 1982, 2,
- 7 R. H. Davis, J. Fluid Mech., 1984, 145, 179-199.
- 8 K. Grosch and A. Schallamach, Rubber Chem. Technol., 1976, 49, 862-908.
- 9 T.-J. Ji, Y.-f. Gao and R.-S. Chen, J. Traffic Transport. Eng., 2010, 10, 57-60.
- 10 V. Bertin, Z. Zhang, R. Boisgard, C. Grauby-Heywang, E. Raphael, T. Salez and A. Maali, Phys. Rev. Res., 2021, 3, L032007.

- 11 M. H. Essink, A. Pandey, S. Karpitschka, C. H. Venner and J. H. Snoeijer, J. Fluid Mech., 2021, 915.
- 12 B. Saintyves, T. Jules, T. Salez and L. Mahadevan, Proc. Natl. Acad. Sci. U. S. A., 2016, 113, 5847-5849.
- 13 H. P. Evans and R. W. Snidle, *J. Lubr. Technol.*, 1981, 103, 539-546.
- 14 D. Dowson and G. Higginson, J. Mech. Eng. Sci., 1959, 1, 6-15.
- 15 H. Christensen, Proc. R. Soc. London, Ser. A, 1962, 266, 312-328.
- 16 K. Herrebrugh, J. Lubr. Technol., 1970, 92, 292-302.
- 17 K. M. Lee and H. S. Cheng, J. Lubr. Technol., 1973, 95, 308-317.
- 18 R. H. Davis, J.-M. Serayssol and E. Hinch, J. Fluid Mech., 1986, 163, 479-497.
- 19 M. Scaraggi and B. Persson, Tribol. Lett., 2012, 47, 409-416.
- 20 M. Scaraggi, G. Carbone, B. N. Persson and D. Dini, Soft Matter, 2011, 7, 10395-10406.
- 21 B. Persson and M. Scaraggi, J. Phys.: Condens. Matter, 2009, 21, 185002.
- 22 Y. Wang, M. R. Tan and J. Frechette, Soft Matter, 2017, 13, 6718-6729.
- 23 P. Vergne and S. Bair, Tribol. Lett., 2014, 54, 1-12.
- 24 O. Pinkus and B. Sternlicht, Theory of Hydrodynamic Lubrication, Mc-Graw Hill Book Company Inc., New York, 1961.
- 25 K. L. Johnson, Contact Mechanics, Cambridge University Press, Cambridge, 1985.
- 26 Z. He, Z. Liu, M. Li, C.-Y. Hui and A. Jagota, J. R. Soc., Interface, 2021, 18, 175.
- 27 J. Li and T.-W. Chou, Int. J. Solids Struct., 1997, 34, 4463-4478.